Bone Reports 8 (2018) 90–94

Contents lists available at ScienceDirect

Bone Reports

journal homepage: www.elsevier.com/locate/bonr

Decreased osteoprogenitor proliferation precedes attenuation of cancellous bone formation in ovariectomized rats treated with sclerostin antibody

Rogely Waite Boyce[a,*], Danielle Brown[b], Melanie Felx[c], Nacera Mellal[c], Kathrin Locher[a], Ian Pyrah[a,1], Michael S. Ominsky[d,2], Scott Taylor[a]

[a] Department of Comparative Biology and Safety Sciences, Amgen Inc., One Amgen Center Drive, Thousand Oaks, CA 91320, United States
[b] Charles River Laboratories, 4025 Stirrup Creek Drive, Suite 150, Durham, NC 27703, United States
[c] Charles River Laboratories, 22022 Transcanadienne, Senneville, QC H9X 3R3, Canada
[d] Department of CardioMetabolic Disorders, Amgen Inc., One Amgen Center Drive, Thousand Oaks, CA 91320, United States

ARTICLE INFO

Keywords:
Osteoporosis
Anabolics
Cell signaling
Osteoprogenitors
Wnt signaling
Bone

ABSTRACT

Sclerostin antibody (Scl-Ab) stimulates bone formation, which with long-term treatment, attenuates over time. The cellular and molecular mechanisms responsible for the attenuation of bone formation are not well understood, but in aged ovariectomized (OVX) rats, the reduction in vertebral cancellous bone formation is preceded by a reduction in osteoprogenitor (OP) number and significant induction of signaling pathways known to suppress mitogenesis and cell cycle progression in the osteocyte (OCy) (Taylor et al., 2016). To determine if the reduction in OP number is associated with a decrease in proliferation, aged OVX rats were administered vehicle or Scl-Ab for 9 or 29 days and implanted with continuous-delivery 5-bromo-2′-deoxyuridine (BrdU) mini-osmotic pumps 5 days prior to necropsy. The total number of BrdU-labeled osteoblasts (OB) was quantified in vertebral cancellous bone to indirectly assess the effects of Scl-Ab treatment on OP proliferation at the time of activation of modeling-based bone formation at day 9 and at the time of maximal mineralizing surface, initial decrease in OP number, and transcriptional changes in the OCy at day 29. Compared with vehicle, Scl-Ab resulted in an increase in the total number of BrdU-positive OB (+260%) at day 9 that decreased with continued treatment (+50%) at day 29. These differences in proliferation occurred at time points when the increase in total OB number was significant and similar in magnitude. These findings suggest that reduced OP proliferation contributes to the decrease in OP numbers, an effect that would limit the OB pool and contribute to the attenuation of bone formation that occurs with long-term Scl-Ab treatment.

1. Introduction

Sclerostin antibody (Scl-Ab) stimulates bone formation, largely by increasing modeling-based bone formation on cancellous and cortical bone surfaces (Boyce et al., 2017; Ominsky et al., 2017a; Ominsky et al., 2014). The increase in bone formation is transient, with bone formation attenuating with long-term treatment. The progressive decline in bone formation in response to Scl-Ab displays envelope-specific behavior. In rats and monkeys administered Scl-Ab, bone formation attenuates first on the cancellous bone surfaces, followed by a more delayed attenuation on the cortical surfaces (Chouinard et al., 2016; Li et al., 2014; Ominsky et al., 2017b).

The cellular and molecular basis of the progressive decline in bone formation with long-term Scl-Ab treatment is not completely understood. In rats, long-term Scl-Ab treatment and the progressive decrease in cancellous bone formation is associated with decreases in total number of osteoprogenitors (OP) in the vertebrae (Ominsky et al., 2015; Taylor et al., 2016). In aged ovariectomized (OVX) rats treated

Abbreviations: ANOVA, analysis of variance; BrdU, 5-bromo-2′-deoxyuridine; CDKN1A, cyclin-dependent kinase inhibitor 1A; CDKN2A, CDKN inhibitor 2A; CE, coefficient of error; CV, coefficient of variation; D, day; E2F1, E2F transcription factor 1; FOXM1, Forkhead box protein M1; MS/BS, mineralizing surface per bone surface; MYC, v-myc avian myelocytomatosis viral oncogene homolog; MYCN, MYC neuroblastoma-derived homolog; OB, osteoblast(s); Ob.N, OB number; OCy, osteocyte(s); OP, osteoprogenitor(s); OVX, ovariectomized; PROBE, precision range of an optimally balanced estimator; RB1, retinoblastoma protein 1; RUNX2, Runt-related transcription factor 2; Scl-Ab, sclerostin antibody; Scl-AbVI, 50 mg/kg of a Scl-Ab; SURS, systematic uniform random sampling; TP53, tumor protein p53; VEH, vehicle

* Corresponding author at: Department of Comparative Biology and Safety Sciences, Amgen Inc., One Amgen Center Drive, MS 29-2-A, Thousand Oaks, CA 91320, United States.
E-mail addresses: rboyce@amgen.com (R.W. Boyce), Danielle.Brown@crl.com (D. Brown), Melanie.Felx@crl.com (M. Felx), Nacera.Mellal@crl.com (N. Mellal), kathrinl@amgen.com (K. Locher), ipyrah@seagen.com (I. Pyrah), ominsky@umich.edu (M.S. Ominsky), taylorsc@amgen.com (S. Taylor).
[1] Current address: Seattle Genetics, 21823-30th Drive S.E., Bothell, WA 98021, United States.
[2] Current address: Radius Health, Inc., 950 Winter St, Waltham, MA 02451, United States.

https://doi.org/10.1016/j.bonr.2018.03.001
Received 29 August 2017; Received in revised form 15 February 2018; Accepted 2 March 2018
Available online 03 March 2018

with Scl-Ab for up to 183 days, reduction in OP numbers preceded the reduction in osteoblast (OB) numbers and attenuation of bone formation in vertebral cancellous bone. The initial reduction in OP numbers occurred at the time of maximal bone formation rate and was coincident with significant induction of signaling pathways in the osteocyte (OCy) known to regulate Wnt signaling and suppress mitogenesis and cell cycle progression (Taylor et al., 2016). Induction of these pathways was unique to the OCy and was not observed in the OB or lining cell, other terminally differentiated, nonproliferating cells of the OB lineage (Taylor et al., 2016).

It is unknown if the reduction in OP numbers in cancellous bone marrow is temporally associated with reduced OP proliferation, an effect that would reduce the OB pool and potentially contribute to the progressive attenuation of bone formation with Scl-Ab. To assess the effects of Scl-Ab on OP proliferation, we used 5-bromo-2′-deoxyuridine (BrdU) labeling to quantify total number of BrdU-labeled OB in lumbar vertebral cancellous bone as an indirect assessment of OP proliferation in response to Scl-Ab. Analyses were conducted early in the course of treatment at the time of activation of modeling-based bone formation and later at the time corresponding to the initial decrease in OP numbers, maximal mineralizing surface, and transcriptional changes in the OCy.

2. Materials and methods

2.1. Study design

Six-month-old female Sprague-Dawley rats (SD®IGS; Charles River Laboratories, Raleigh, NC, USA) were OVX and left untreated for 8 weeks. Rats were assigned to four treatment groups in a manner to achieve body weight balance across the treatment groups. Rats were administered vehicle (VEH) or 50 mg/kg of Scl-Ab (Scl-AbVI) by weekly subcutaneous injection. Scl-AbVI was engineered to be less immunogenic in rats (rat fragment crystallizable construct) by modifying the murine parent antibody to be more similar to that found in rats.

Two groups received a single dose of VEH (n = 12) or Scl-Ab (n = 11) and were euthanized on day 9, and two groups received four doses of VEH (n = 11) or Scl-Ab (n = 12) and were euthanized on day 29.

Five days prior to the scheduled necropsies, Alzet® pumps (Model 2ML1 with an infusion rate of 10 µL/h; Cupertino, CA, USA), each containing 2 mL of BrdU at 50 mg/mL in Dulbecco's phosphate buffered saline and 15% dimethyl sulfoxide, were implanted subcutaneously in the interscapular area of all rats. For a rat weighing 500 g, the estimated daily dose of BrdU was 24 mg/kg. Pumps were weighed before and after filling and after removal at necropsy to verify the delivery. Two animals were excluded from subsequent analyses (one day 29 VEH and one day 9 Scl-Ab) due to evidence of pump failure. For euthanasia, animals were anesthetized with isoflurane/oxygen and then exsanguinated. The 5-day labeling period was chosen because it approximates the estimated transit time from OP to mature OB (approximately 7 days) based on lineage-tracing studies in Sox9creER^{T2}, Rosa26-tdTomato, osteocalcin–green fluorescent protein triple-transgenic mice (Kronenberg and Balani, 2015).

The in-life phase of this study was conducted at Charles River Laboratories (Montreal ULC, Canada). Animals were cared for in accordance with the Guide for the Care and Use of Laboratory Animals, 8th Edition (Committee for the Update of the Guide of the Care and Use of Laboratory Animals: National Research Council (US), 2011). All research protocols were approved by the Institutional Animal Care and Use Committee. Animals were group-housed (two per cage) at an Association for Assessment and Accreditation of Laboratory Animal Care, internationally accredited facility, in plastic cages and then transferred to sterile, ventilated, micro-isolator housing with corncob bedding following implantation of Alzet® pumps. Animals had ad libitum access to pelleted feed (Certified Rodent Chow No. 5CR4 [14% protein]; PMI Nutrition International, St. Louis, MO, USA) and water (reverse osmosis purified) using an automatic watering system. Animals were maintained on a 12:12 hour light:dark cycle in rooms with controlled temperature (19°–25 °C) and humidity (30%–70%) and access to enrichment opportunities (hiding tube and a chewing object). Further details on animal care and surgical procedures are provided in Supplementary materials.

2.2. Estimation of total number of BrdU-labeled OB

At necropsy, lumbar vertebrae L1-L2 were isolated and cleaned of the soft tissue; vertebral body segment was isolated, fixed in 10% neutral buffered formalin, and transferred to 70% ethanol. A segment of the duodenum was collected and processed routinely in paraffin to use as a positive control to verify BrdU incorporation. The vertebral segments were decalcified in modified Kristensen's solution, processed in filtered paraffin, and embedded longitudinally in paraffin blocks.

At days 9 and 29 in this study, the total number of BrdU-labeled OB was quantified in vertebral cancellous bone. For quantification, the stereological estimator, the physical fractionator (Gundersen, 1986), was used. Using a random starting point, serial pairs of 3-µm thick sections (physical disectors) were collected, spaced 240 µm apart, by systematic uniform random sampling (SURS), yielding approximately 8–10 disector pairs per animal. Because stereological analyses required exhaustive sectioning of the sample and generation of thin serial section pairs, vertebrae were decalcified to facilitate sectioning and avoid section artifacts, and thus, osteoid surfaces or fluorochrome labeling could not be used to identify active forming surfaces. Therefore, to identify BrdU-labeled OB active in matrix synthesis, a double immunohistochemical staining was performed to colocalize BrdU-positive nuclei in osteonectin-positive OB lining the cancellous bone surface (Fig. 1).

For immunostaining, disector pairs were retrieved offline in Diva Decloaker (Biocare Medical, Concord, CA, USA) for 18 h, rinsed, incubated with 3% H_2O_2 for 10 min, rinsed with buffer, and then transferred to a Ventana Discovery XT (Ventana Medical Systems, Inc., Tucson, AZ, USA). The BrdU immunoreactivity was detected by incubating with an anti-BrdU antibody for 1 h (ab1893; Abcam, Cambridge, MA, USA), followed by biotin-conjugated rabbit antisheep secondary antibody for 32 min (item number 313-065-003; Jackson ImmunoResearch Laboratories, West Grove, PA, USA), and then horseradish peroxidase–labeled streptavidin for 16 min followed by

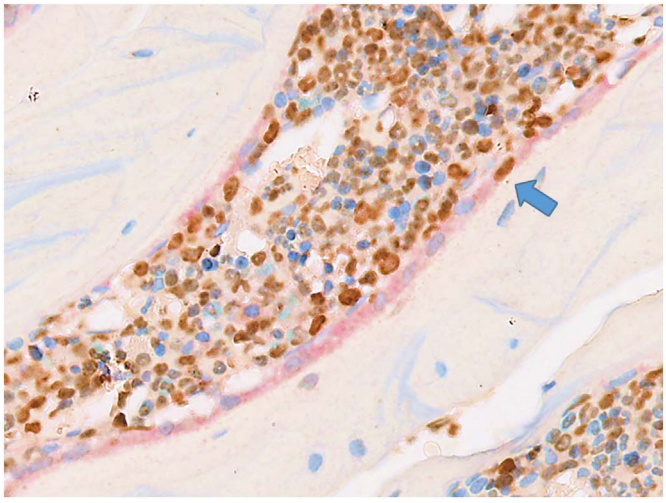

Fig. 1. Double immunohistochemical staining for osteonectin and BrdU to identify BrdU-positive osteoblasts active in matrix synthesis. Osteonectin-positive osteoblasts stained with Fast Red line the cancellous bone surfaces in a Scl-Ab–treated rat, with a BrdU-positive osteoblast (blue arrow, original magnification 400×). BrdU = 5-bromo-2′-deoxyuridine; Scl-Ab = sclerostin antibody.

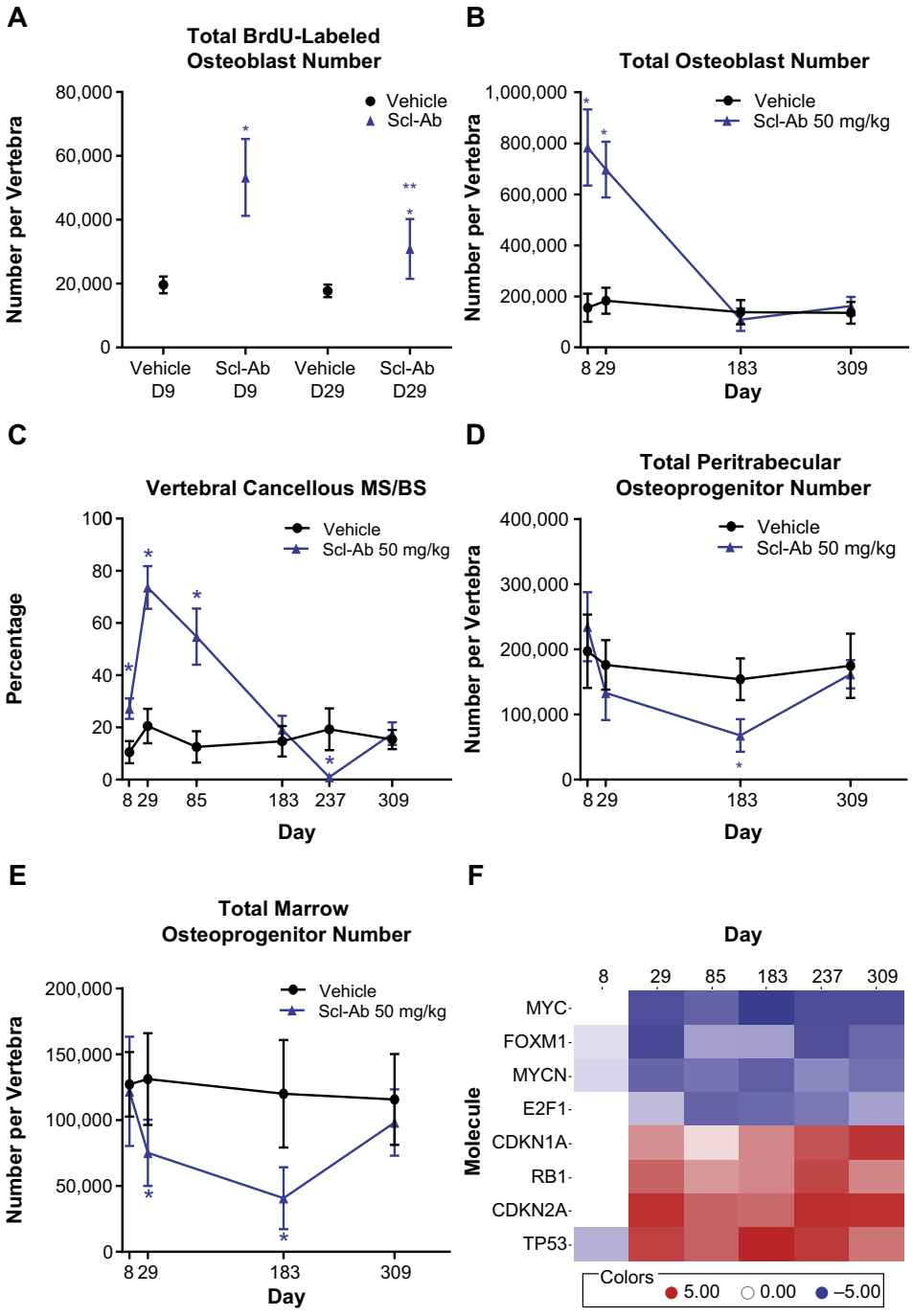

Fig. 2. Time-dependent effects of Scl-Ab on rat vertebral cancellous bone osteoblast and osteoprogenitor populations and osteocyte signaling pathways. (A) Total number of BrdU-positive osteoblasts at day 9 and day 29, (B) total osteoblast number, (C) cancellous mineralizing surface, (D) total peritrabecular osteoprogenitor number, (E) total marrow osteoprogenitor number, and (F) heat map of activation status of signaling pathways related to mitogenesis and cell cycle progression in the osteocyte based on an upstream regulator analysis (red indicates activation and blue indicates inhibition) in aged ovariectomized rats administered Scl-Ab through day 183, followed by a treatment-free period through day 309, modified from Taylor et al. (Taylor et al., 2016). See Taylor et al. (Taylor et al., 2016) for additional experimental details. Values shown are mean ± standard deviation. *$p \leq 0.05$, 2-way analysis of variance, *t*-test, or Sidak's multiple comparison test, compared with vehicle. **$p \leq 0.05$, Scl-Ab day 9 vs day 29. BrdU = 5-bromo-2′-deoxyuridine; CDKN1A = cyclin-dependent kinase inhibitor 1A; CDKN2A = CDKN inhibitor 2A; D = day; E2F1 = E2F transcription factor 1; FOXM1 = Forkhead box protein M1; MS/BS = mineralizing surface per bone surface; MYC = v-myc avian myelocytomatosis viral oncogene homolog; MYCN = MYC neuroblastoma-derived homolog; RB1 = retinoblastoma protein 1; Scl-Ab = sclerostin antibody; TP53 = tumor protein p53.

diaminobenzadine for 8 min. Osteonectin immunoreactivity was detected by incubating with anti-osteonectin antibody for 1 h (item number 1 21420; Thermo Fisher Scientific, Waltham, MA, USA), followed by biotin-conjugated goat antimouse antibody for 32 min (item number 115 066-003; Jackson ImmunoResearch Laboratories), and then alkaline phosphatase–labeled streptavidin for 16 min followed by Fast Red for 8 min. Sections were counterstained with hematoxylin.

Slides were scanned with a digital slide scanner and the image files were imported into the AutoDisector™ platform of the Visiopharm® software (Visiopharm, Høsersholm, Denmark). Superimages of disector pairs were created, linked, and aligned, and the region of interest was defined manually. Only cancellous bone within the vertebral bodies was included in the region of interest. Matching virtual 40× objective magnification fields were sampled from disectors by SURS with an area-sampling fraction of 4%. Two independent samplings were performed for all animals.

Sampled fields were loaded into the NewCAST™ (Visiopharm) platform of the Visiopharm® software, and BrdU-positive OB along the bone surface (plump cells that were positive for both osteonectin and BrdU staining) were counted manually using a 200 µm × 200 µm unbiased counting frame detailed by Gundersen (Gundersen, 1977). The counting was performed using the disector counting principle (Sterio, 1984) in both directions of the disector pair using the nucleus as the unique counting feature.

The number of cells counted for the duplicate samplings was averaged for each animal. The average was then divided by 2 (to correct for counting performed in both directions of the disector) and then multiplied by the inverse of the sampling fractions to obtain the final estimate of total cell count. All final estimates were divided by 2 to express number per vertebra, as both L1-L2 were counted. The coefficient

of error (CE) was calculated for each animal according to Løkkegaard (Løkkegaard, 2004). The mean number estimate, standard deviation, mean CE, and coefficient of variation (CV) were then calculated for each group.

The mean CE and CV for each group were used to estimate the precision of the estimator using the precision range of an optimally balanced estimator (PROBE) equation: CV^2 / CE^2. A design is considered optimal if the results of the equation are between 2 and 4, and it is too imprecise if the result is < 2 (Gundersen et al., 2013).

The results of the estimation using PROBE equation are presented below and indicate that the estimation method had sufficient precision.

Study day	Average CE	Average CV	PROBE result
9	0.09	0.18	4.0
29	0.11	0.21	3.6

The PROBE equation result for each study day was > 2, indicating that the estimates were of adequate precision.

To compare the time-dependent effects of Scl-Ab on total number of BrdU-labeled OB as an index of OP proliferation to temporal changes in indices of surface extent of bone formation (total OB number [Ob.N] and mineralizing surface per bone surface [MS/BS]), OP numbers, and gene expression in the OCy, results were included from a previous study in aged OVX rats administered either VEH or weekly Scl-AbVI for 183 days followed by a treatment-free period (Taylor et al., 2016).

2.3. Statistical analyses

To assess the significance of treatment, time, and treatment-by-time interaction effects at the 5% level, a two-way analysis of variance (ANOVA) model was fit separately to the total number of BrdU-labeled OB data using SAS v9.2 (SAS Institute, Cary, NC, USA). Given that in all cases, the interaction factor was found to be significant, the treatment levels were also compared within each of the two time points (day 9 and 29) using a *t*-test. No adjustments for multiple comparison were necessary, as there was only one comparison for each of the two factors considered (group and day) in the ANOVA model. For Ob.N, MS/BS, and OP numbers, a two-way ANOVA followed by Sidak's multiple comparisons test for comparison of Scl-Ab with VEH was performed using GraphPad Prism® v6.05 (GraphPad Software, Inc., La Jolla, CA, USA).

3. Results

The total number of BrdU-labeled OB was significantly increased with Scl-Ab at day 9 by approximately 260% and at day 29 by approximately 50% compared with the concurrent VEH controls, with significant treatment, time, and treatment-by-time interaction (Fig. 2A). Although the total number of BrdU-labeled OB remained increased at day 29 with Scl-Ab treatment, it was significantly reduced compared with day 9. These effects on BrdU-labeled OB occurred when Ob.N was significantly increased (Fig. 2B). The estimated percentage of BrdU-labeled OB was approximately 13.6% at day 9 and 8.8% at day 29 based on mean values.

The reduction in total number of BrdU-labeled OB occurred when MS/BS was maximal (Fig. 2C) and was coincident with reduction in OP numbers (Fig. 2D and E) and a transcriptional switch in the OCy, consistent with cell cycle arrest (Fig. 2F). As bone formation decreased to control levels at day 183, OP numbers were further decreased whereas the transcriptional signature in the OCy persisted.

4. Discussion

Using the total number of BrdU-labeled OB in vertebral cancellous bone as an indirect assessment of OP proliferation, we have shown that in aged OVX rats, Scl-Ab results in an increase in OP proliferation early in the course of treatment at day 9. At day 29, OP proliferation decreased compared with day 9. At both days 9 and 29, bone formation was significantly increased, supported by the marked increased in Ob.N. The decrease in OP proliferation at day 29 occurred at the time of peak MS/BS, prior to attenuation of bone formation, and was coincident with a decline in Runt-related transcription factor 2 (RUNX2)–labeled OP numbers and regulation of pathways that would limit mitogenesis and cell cycle progression in the OCy (Taylor et al., 2016).

An increase in OP proliferation at day 9 was not unexpected because of the high demand for OB to support modeling-based bone formation that increased from approximately 7% to 63% on vertebral cancellous bone surfaces in the aged OVX rats in response to Scl-Ab, following 5 weeks of treatment (Ominsky et al., 2014). An increase in total OP number labeled using Sox9creER^{T2} Rosa26-tdTomato transgenic mice was shown after 9 days of treatment with a Scl-Ab in whole vertebral bodies using tissue-clearing methods and light sheet microscopy (Greenbaum et al., 2017). These data are consistent with the increase in number of BrdU-labeled OB in the current rat study. Although activation of quiescent bone-lining cells contributes to the early increase in modeling-based formation with Scl-Ab in cortical bone (Kim et al., 2017), these data indicate that by day 9, there is also recruitment of new OB to the bone surface derived from a proliferating OP population to sustain bone formation. Both of these mechanisms could contribute to the marked increase in Ob.N at day 9. A corresponding increase in MS/BS was not observed at day 9, because much of the bone surfaces were covered with early osteoid seams at this time point (Nioi et al., 2015). An increase in total OP numbers was not observed at day 8 using RUNX2 immunohistochemistry, morphology, and location to identify OP subpopulations and stereological analyses in Scl-Ab–treated aged OVX rats (Taylor et al., 2016). The failure to detect an acute increase in OP numbers in the rat study may be a reflection of the higher dose of Scl-Ab used in the mouse study, differences in the quantified OP populations, or differences in the sensitivity of the quantitation methods.

A decrease in OP proliferation at day 29 relative to day 9 with Scl-Ab was noteworthy because the demand for OB remained high at day 29. This was the time point of maximal MS/BS and high Ob.N in Scl-Ab–treated rats. However, both BrdU-labeled OB and OP numbers decreased. These combined effects at day 29 possibly suggest that to meet the demand for OB on the bone surface, under conditions of reduced OP proliferation, OP that escaped a replication cycle were recruited to the bone surface, leading to a reduction in OP numbers in the marrow. These effects on OP proliferation were likely sustained with continued dosing, because OP numbers continued to decrease as bone formation attenuated (Taylor et al., 2016). In contrast with Scl-Ab, intermittent human parathyroid hormone (1–34), another anabolic agent, was not associated with a reduction in OP numbers and did not display a progressive decrease in bone formation with chronic treatment in rats (Ominsky et al., 2015).

An interesting observation was that the decrease in OP proliferation and initial reduction in OP numbers occurred coincident with the onset of a transcriptional signal in the OCy, consistent with cell cycle arrest. In addition, OP numbers continued to decrease as bone formation attenuated with continued Scl-Ab dosing while this signal persisted in the OCy. The relationship of this transcriptional signature to changes in the OP populations is unknown. Cell cycle arrest signal would not be anticipated in a terminally differentiated cell such as the OCy. However, the OCy could possibly communicate this signal to the OP populations as data support that the OCy can regulate hematopoiesis and progenitor mobilization (Asada and Katayama, 2014; Kamioka et al., 2001) potentially by exosome/microvesicle transfer (Kamel-ElSayed et al., 2015; Wang et al., 2014). Alternatively, the OCy signature may reflect transcriptional plasticity as has been demonstrated for the OCy under certain conditions, potentially sharing a transcriptional pattern with the OP population (Qing et al., 2012). Further studies with isolated OP cells are required where transcriptional profiles can be compared to the OCy.

There are several limitations to this study. OP proliferation was not directly evaluated; rather, it was inferred from BrdU labeling in the OB. The lack of robust phenotypic markers for rat OP limits the evaluation of the OP population. RUNX2 is a robust marker of the entire OB lineage. We previously used RUNX2 immunoreactivity along with morphological criterion and location to estimate the number of specific OP populations in rat vertebrae (Ominsky et al., 2015; Taylor et al., 2016). Immunohistochemical detection of RUNX2 results in a nuclear signal, and colocalization with the nuclear signal for BrdU, whether by fluorescent or chromogenic detection, to identify proliferating OP populations is problematic with the stereology platform camera interface and application of the automated physical fractionator. In addition, the methods used in this study could not assess the effects of treatment on OP transit time, another possible factor that could influence the number of BrdU-labeled OB on the bone surface and the number of OP. A time-course lineage-tracing study in transgenic mice would be required to directly assess the effects of Scl-Ab on OP proliferation and transit time.

In summary, using number of BrdU-labeled OB to index OP proliferation, Scl-Ab resulted in an early transient increase in OP proliferation coincident with the activation of modeling-based bone formation. At the time of peak MS/BS and prior to the attenuation of bone formation, OP proliferation remained increased relative to VEH but decreased compared with the earlier time point. The decrease in proliferation occurred coincident with decreases in OP numbers, even though bone formation remained significantly increased and temporally associated with the onset of transcriptional changes in the OCy, consistent with suppression of mitogenesis and cell cycle progression. Collectively, these data suggest that reduced OP proliferation contributes to the progressive decrease in bone formation that occurs with long-term Scl-Ab treatment.

Transparency document

The http://https/dx.doi.org/10.1016/j.bonr.2018.03.001 associated with this article can be found in the online version.

Conflict of interest statement

RWB, KL, IP, and MSO are former Amgen Inc. employees; MSO holds Amgen Inc. stock. DB, MF, and NM are employees of Charles River Laboratories. ST is an employee of Amgen Inc. and owns Amgen Inc. stock and/or stock options.

Funding source

This work was supported by Amgen Inc. and UCB Pharma.

Acknowledgments

The authors are grateful to Gurpreet Kaur of CACTUS Communications (on behalf of Amgen Inc.) and Amy Foreman-Wykert, PhD, of Amgen Inc. for editing and formatting the manuscript.

Authors' roles

All authors participated in the design or implementation of the study and/or the analysis or interpretation of the findings and had access to the study data. All authors contributed to the development and critical revision of the manuscript and approved the final version for submission. RWB, DB, MF, NM, and ST take responsibility for the integrity of the data analysis.

Appendix A. Supplementary data

Supplementary data to this article can be found online at https://doi.org/10.1016/j.bonr.2018.03.001.

References

Asada, N., Katayama, Y., 2014. Regulation of hematopoiesis in endosteal microenvironments. Int. J. Hematol. 99 (6), 679–684.
Boyce, R.W., Niu, Q.T., Ominsky, M.S., 2017. Kinetic reconstruction reveals time-dependent effects of romosozumab on bone formation and osteoblast function in vertebral cancellous and cortical bone in cynomolgus monkeys. Bone 101, 77–87.
Chouinard, L., Felx, M., Mellal, N., Varela, A., Mann, P., Jolette, J., Samadfam, R., Smith, S.Y., Locher, K., Buntich, S., Ominsky, M.S., Pyrah, I., Boyce, R.W., 2016. Carcinogenicity risk assessment of romosozumab: a review of scientific weight-of-evidence and findings in a rat lifetime pharmacology study. Regul. Toxicol. Pharmacol. 81, 212–222.
Committee for the Update of the Guide of the Care and Use of Laboratory Animals: National Research Council (US), 2011. Guide for the Care and Use of Laboratory Animals. National Academies Press (US), Washington, DC.
Greenbaum, A., Chan, K., Dobreva, T., 2017. Bone CLARITY: clearing, imaging, and computational analysis of osteoprogenitors within intact bone marrow. Sci. Transl. Med. 9 (387), eaah6518.
Gundersen, H.J.G., 1977. Notes on the estimation of the numerical density of arbitrary profiles: the edge effect. J. Microsc. 111 (2), 219–223.
Gundersen, H.J., 1986. Stereology of arbitrary particles. A review of unbiased number and size estimators and the presentation of some new ones, in memory of William R. Thompson. J. Microsc. 143 (Pt 1), 3–45.
Gundersen, H.J.G., Mirabile, R., Brown, D., Boyce, R.W., 2013. Stereological principles and sampling procedures for toxicologic pathologists. In: Haschek, W.M., Rousseaux, C.G., Wallig, M.A. (Eds.), Haschek and Rousseaux's Handbook of Toxicologic Pathology. Elsevier, Inc., Academic Press, Waltham, MA, pp. 263–265.
Kamel-ElSayed, S.A., Tiede-Lewis, L.M., Lu, Y., Veno, P.A., Dallas, S.L., 2015. Novel approaches for two and three dimensional multiplexed imaging of osteocytes. Bone 76, 129–140.
Kamioka, H., Honjo, T., Takano-Yamamoto, T., 2001. A three-dimensional distribution of osteocyte processes revealed by the combination of confocal laser scanning microscopy and differential interference contrast microscopy. Bone 28 (2), 145–149.
Kim, S.W., Lu, Y., Williams, E.A., Lai, F., Lee, J.Y., Enishi, T., Balani, D.H., Ominsky, M.S., Ke, H.Z., Kronenberg, H.M., Wein, M.N., 2017. Sclerostin antibody administration converts bone lining cells into active osteoblasts. J. Bone Miner. Res. 32 (5), 892–901.
Kronenberg, H.M., Balani, D., 2015. Parathyroid hormone administration regulates osteoprogenitor numbers and decreases their differentiation into the adipocytic lineage *in vivo*. J. Bone Miner. Res. 30 (Suppl. 1).
Li, X., Niu, Q.T., Warmington, K.S., Asuncion, F.J., Dwyer, D., Grisanti, M., Han, C.Y., Stolina, M., Eschenberg, M.J., Kostenuik, P.J., Simonet, W.S., Ominsky, M.S., Ke, H.Z., 2014. Progressive increases in bone mass and bone strength in an ovariectomized rat model of osteoporosis after 26 weeks of treatment with a sclerostin antibody. Endocrinology 155 (12), 4785–4797.
Løkkegaard, A., 2004. The number of microvessels estimated by an unbiased stereological method applied in a brain region. In: Evans, S.M., Janson, A.M., Nyengaard, J.R. (Eds.), Quantitative Methods in Neuroscience: A Neuroanatomical Approach. Oxford University Press, Oxford, England, pp. 178.
Nioi, P., Taylor, S., Hu, R., Pacheco, E., He, Y.D., Hamadeh, H., Paszty, C., Pyrah, I., Ominsky, M.S., Boyce, R.W., 2015. Transcriptional profiling of laser capture microdissected subpopulations of the osteoblast lineage provides insight into the early response to sclerostin antibody in rats. J. Bone Miner. Res. 30 (8), 1457–1467.
Ominsky, M.S., Niu, Q.T., Li, C., Li, X., Ke, H.Z., 2014. Tissue-level mechanisms responsible for the increase in bone formation and bone volume by sclerostin antibody. J. Bone Miner. Res. 29 (6), 1424–1430.
Ominsky, M.S., Brown, D.L., Van, G., Cordover, D., Pacheco, E., Frazier, E., Cherepow, L., Higgins-Garn, M., Aguirre, J.I., Wronski, T.J., Stolina, M., Zhou, L., Pyrah, I., Boyce, R.W., 2015. Differential temporal effects of sclerostin antibody and parathyroid hormone on cancellous and cortical bone and quantitative differences in effects on the osteoblast lineage in young intact rats. Bone 81, 380–391.
Ominsky, M.S., Boyce, R.W., Li, X., Ke, H.Z., 2017a. Effects of sclerostin antibodies in animal models of osteoporosis. Bone 96, 63–75.
Ominsky, M.S., Boyd, S.K., Varela, A., Jolette, J., Felx, M., Doyle, N., Mellal, N., Smith, S.Y., Locher, K., Buntich, S., Pyrah, I., Boyce, R.W., 2017b. Romosozumab improves bone mass and strength while maintaining bone quality in ovariectomized cynomolgus monkeys. J. Bone Miner. Res. 32 (4), 788–801.
Qing, H., Ardeshirpour, L., Pajevic, P.D., Dusevich, V., Jahn, K., Kato, S., Wysolmerski, J., Bonewald, L.F., 2012. Demonstration of osteocytic perilacunar/canalicular remodeling in mice during lactation. J. Bone Miner. Res. 27 (5), 1018–1029.
Sterio, D.C., 1984. The unbiased estimation of number and sizes of arbitrary particles using the disector. J. Microsc. 134 (Pt 2), 127–136.
Taylor, S., Ominsky, M.S., Hu, R., Pacheco, E., He, Y.D., Brown, D.L., Aguirre, J.I., Wronski, T.J., Buntich, S., Afshari, C.A., Pyrah, I., Nioi, P., Boyce, R.W., 2016. Time-dependent cellular and transcriptional changes in the osteoblast lineage associated with sclerostin antibody treatment in ovariectomized rats. Bone 84, 148–159.
Wang, K., Keightley, A., Veno, P., Dusevich, V., Tiede-Lewis, L., Bonewald, I., Dallas, S.L., 2014. Osteocyte microvesicles in cell–cell communication in bone. J. Bone Miner. Res. 29 (Suppl. 1).